Journal of Quantitative Spectroscopy & Radiative Transfer 221 (2018) 98–109

Contents lists available at ScienceDirect

Journal of Quantitative Spectroscopy & Radiative Transfer

journal homepage: www.elsevier.com/locate/jqsrt

Performance of the discrete dipole approximation for optical properties of black carbon aggregates

Chao Liu[a,b,*], Shiwen Teng[a,b], Yingying Zhu[a,b], Maxim A. Yurkin[c,d], Yuk L. Yung[e]

[a] Collaborative Innovation Center on Forecast and Evaluation of Meteorological Disasters, Nanjing University of Information Science & Technology, Nanjing 210044, China
[b] Key Laboratory for Aerosol-Cloud-Precipitation of China Meteorological Administration, School of Atmospheric Physics, Nanjing University of Information Science & Technology, Nanjing 210044, China
[c] Voevodsky Institute of Chemical Kinetics and Combustion SB RAS, Institutskaya str. 3, Novosibirsk 630090, Russia
[d] Novosibirsk State University, Pirogova 2, Novosibirsk 630090, Russia
[e] Division of Geological and Planetary Sciences, California Institute of Technology, Pasadena, CA 91125, USA

ARTICLE INFO

Article history:
Received 5 September 2018
Revised 28 September 2018
Accepted 29 September 2018
Available online 1 October 2018

Keywords:
Black carbon aggregate
Discrete-dipole approximation
Effective medium approximation

ABSTRACT

The optical properties of black carbon (BC) are fundamental for radiative transfer and remote sensing. BC geometry is successfully represented by an idealized model named "fractal aggregate", and numerous methods are available and widely used to simulate the corresponding optical properties. This study systematically evaluates the performance of the discrete dipole approximation (DDA) for optical simulations of BC aggregates. The Multiple Sphere T-Matrix (MSTM) results are used as references for accuracy evaluation. The differences between the DDA and MSTM can be controlled to be less than 3% by using dipole size much smaller than the monomer size, and the DDA efficiency is sensitive to aggregate structures, e.g. lacy or compact. We find that shape representation for small-sized monomers during DDA discretization leads significant errors, i.e., up to 10%, and relatively large refractive index of BC also affects the DDA accuracy. However, the MSTM treats the BC monomers as perfect spheres without overlapping, and the imperfect structure that is implicitly introduced in the DDA simulations due to the spatial discretization may be a better representation of realistic BC particles. Moreover, the accuracy and efficiency of the DDA can be improved by defining dipoles on the particle boundary to have refractive indices given by the effective medium approximation (EMA). This leads to the adequate shape representation even using larger dipole sizes, and results in the DDA accuracy comparable to that of the reference MSTM solution.

1. Introduction

Black carbon (BC), produced by incomplete combustion, is one of the most significant contributors to global warming due to its strong absorption of solar radiation [1]. It plays an important role in the radiative forcing at regional and global scales, and may enhance the occurrence of extreme haze pollution episodes by inducing heating in the planetary boundary layer [2]. Thus, the optical properties of BC aerosol are fundamental for a better understanding of its radiative effects and remote sensing studies.

BC particles normally exist as aggregates of spherical monomers [3,4], and fractal geometry is used for describing BC complex morphologies [5–7]. Mathematically, the parameters that describe fractal aggregates are related by [5]:

$$N = k_f \left(\frac{R_g}{a}\right)^{D_f}. \quad (1)$$

Here, N is the number of monomers in an aggregate, and a is the monomer radius. The gyration radius R_g quantifies the spreads of the monomers. The fractal prefactor k_f and fractal dimension D_f are two important parameters describing the compactness of an aggregate. Relatively compact aggregates with a fixed N and a have smaller R_g, so require a larger D_f or k_f to satisfy the relationship in Eq. (1).

With geometries based on the fractal aggregate rigorously defined, accurate simulations of BC optical properties become possible. Numerous numerical models are developed and applied to account for the optical properties of BC aggregates [8–10]. Among the existing methods, the Multiple Sphere T-Matrix method (MSTM) [8,11] and the Generalized Multi-particle Mie (GMM) method [12,13] are specially designed for scattering properties of multiple spheres. Both the MSTM and GMM can only consider aggre-

* Corresponding author at: School of Atmospheric Physics, Nanjing University of Information Science & Technology, Nanjing 210044, China.
E-mail address: chao_liu@nuist.edu.cn (C. Liu).

https://doi.org/10.1016/j.jqsrt.2018.09.030
0022-4073/

Table 1
Comparison of the previous studies using the DDA to calculate optical properties of BC aggregates.

Reference	Refractive index[a]	Size			dpl[c]	RE[d]
		N	Monomer size[b]	Coating size[b]		
Kahnert et al. [22]	1.76 + 0.63i	4–1600	0.15	1.0–6.0	~ 40	<3%
Prasanna et al. [23]	2.5 + 1.5i	2	0.01	0	3000–6000	3%–8%
Prasanna et al. [23]	2.2 + 1.3i	20–100	0.024	0	~1000	~20%
Wu et al. [24]	1.76 + 0.57i	200	0.17	~2.8	~ 150–800	8%–1%
Moteki [25]	1.75 + 0.44i	1	0.05–0.5	0	Not given	<20%
Liu et al. [26]	1.73 + 0.59i	200	0.17	1.0	80	~3%
Doner et al. [27]	1.75 + 0.63i	200	0.12–0.29	0	110–255	8%
Tazaki & Tanaka [28]	3.4 + 0.05i	64	0.0006–0.6	0	~50–50,000	33%–1%

[a] Refractive index of black carbon aerosols when coating material is also present.
[b] The size is given as the size parameter.
[c] Number of dipoles per wavelength (see text).
[d] The relative errors of the integral scattering properties (extinction or absorption) by comparing with MSTM.

gates of perfect spheres without overlapping. Meanwhile, more general methods that are applicable for particles with arbitrary geometries can also calculate BC optical properties, such as the discrete dipole approximation (DDA) [14,15] and finite difference time domain method (FDTD) [16]. The geometric-optics method has also been extended and improved to account for optical properties of aggregates by considering surface wave [17,18]. A well-chosen method may not only save significant computational resources but also provide more robust and accurate results, whereas an inappropriate method may draw misleading or wrong conclusions. Therefore, a complete and rigorous understanding on the performance of different numerical methods themselves is needed.

Among those numerical models, the DDA solves the electromagnetic integral equation in the frequency domain, and has been extensively applied to investigate aggregate optical properties, especially those with irregular or inhomogeneous geometries [19–21]. In the framework of the DDA, a particle is discretized into small sub-volumes (namely dipoles), and interactions derived from the aforementioned integral equation can be approximated by those among point dipoles. Thus, the DDA is fully flexible on particle geometries. Considering that the MSTM or GMM can only be applied to fractal aggregates of perfect spheres without overlapping [11–12], the DDA is widely used to investigate the effects of more realistic monomer irregularity, e.g., overlapping, necking, and coating, on BC optical properties [19–28]. During the application of the DDA, those studies either briefly evaluate the DDA for BC aggregate applications [22–28], or directly carry out the DDA simulations for their particular applications without validation [29–31].

Table 1 summarizes some of the previous studies that include discussions on the DDA performance [22–28]. Most of these studies use the DDA for their particular applications related to aggregate optical properties, and the DDA is evaluated only briefly. As another rigorous solution of the Maxwell equations, the MSTM solves equations in the multiple spherical boundary domain, so it is often used as the reference method for the evaluations of other methods. Table 1 lists some key parameters used for the DDA, i.e., refractive index, particle sizes, and spatial resolution used, and the last column is the relative errors (REs) of the DDA results (mostly for the cross sections), which range between over 30% to almost zero. The parameter "dpl", namely dipoles per lambda (wavelength), is widely used in the DDA literature to describe the discretization level. While certain rules-of-thumb exist for satisfactory accuracy, e.g. dpl $\approx 10|m|$, where m is the complex refractive index, they are largely misleading when the particle or some of its structural elements is much smaller than the wavelength [20,32]. This is illustrated by the values of dpl in Table 1. The large variation is not so much due to inherent factors affecting accuracy, but rather due to the varying sizes of the monomer and of the whole aggregate. Still, we continue to use dpl or derived parameters in this paper due to their convenience for labeling different discretization. Overall, there are two factors complicating the application of the DDA for calculating BC aggregate optical properties. First, the performance of the DDA method is challenged if the real part of refractive index becomes relatively large [33]. Second, BC monomers have small size, so the choice of discretization (dpl) becomes critical, especially if both numerical accuracy and efficiency are considered.

Considering the significant uncertainties and demands for the DDA, this study presents a complete and systematic investigation on the performance of the DDA for the aggregate optical simulations, and develops a treatment based on the effective medium approximation to improve the DDA accuracy and efficiency. The paper is organized as follows. Section 2 introduces the DDA method and simulation parameters. The performance of the DDA is discussed in Sections 3, and a treatment based on the effective medium approximation is presented in Section 4 to improve the DDA performance. Section 5 concludes this study.

2. Method

As one of the most widely used numerical solution of light scattering by nonspherical particles, the features of the DDA has been extensively studied for general applications, whereas, typically, the particles are larger than the incident wavelengths. However, this study focuses on a special case of particles with relatively small overall sizes but complex geometries. The ADDA implementation (v1.3) developed by Yurkin and Hoekstra [34–37] is used in this study; it is parallelized with the MPI to be run on computer clusters. Due to the similar default settings and accuracy to another DDA code DDSCAT [36], our results can be understood for the DDA method in general. Some important parameters related to the DDA simulations are introduced in this section.

The DDA discretizes particles into small dipoles, and, for a given particle, its efficiency and accuracy are mostly determined by the dpl used for the simulation. The dipoles should be much smaller than both the incident wavelength and the particle length scale to better represent its geometry. For BC aggregates, typical monomer diameters range between 10 and 100 nm, and we are interested in their optical properties in ultraviolet, visible, or shortwave infrared wavelengths, i.e., in the order of a few hundred nanometers. Thus, the rule-of-thumb dpl value of 10|m| is definitely not sufficient; it should be large enough to adequately represent these small monomers. An alternative parameter describing the dipole size is its size parameter kd, where $k = 2\pi/\lambda$ and d are wavenumber and dipole size, respectively. The two are related as $kd = 2\pi/dpl$.

We use the default DDA formulation in ADDA [37], namely interaction of point dipoles and the lattice dispersion relation

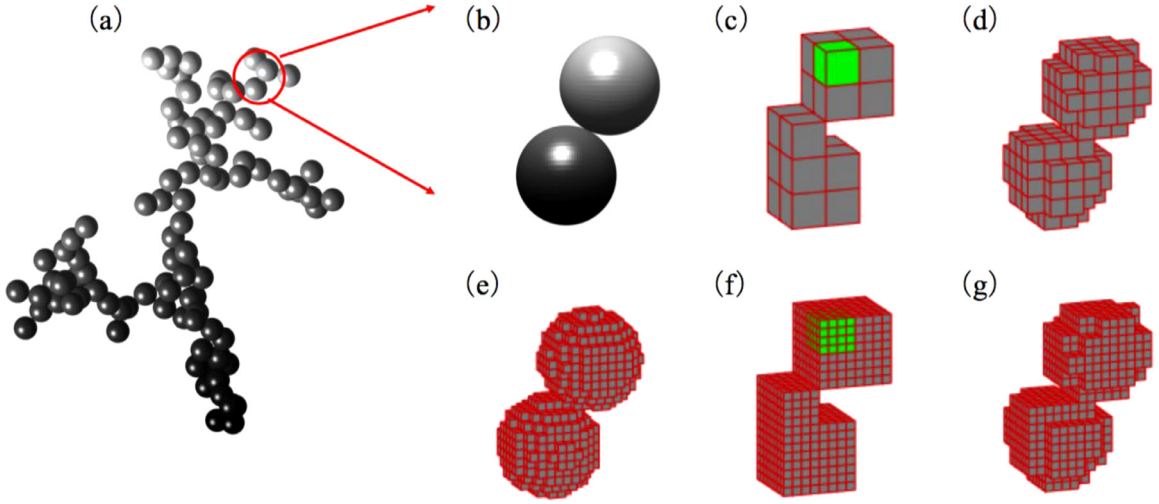

Fig. 1. (a) A fractal aggregate consisting of 100 monomers with the morphological factors of the aggregate $D_f = 1.8$, $k_f = 1.2$, and $a = 15$ nm. (b) Two monomers of the fractal aggregate. (c–e) The discretization geometry with dpl of 50, 100 and 200. (f) The geometry same as (c) but dpl = 200. (g) The geometry same as (d) but dpl = 200.

for polarizability formulation. The latter is not important, since $kd \ll 1$, but different interaction formulations can make a difference. Especially promising for future research is the integration of the Green's tensor (IGT) [38]. The linear system inside the DDA is solved iteratively, for which also the default ADDA parameters are used, namely the quasi minimal residual method with convergence threshold of 10^{-5} [37]. This threshold is good enough to have no noticeable influence on the final DDA accuracy.

The fractal aggregates are generated by a tunable aggregation algorithm [39]. Lacy and compact aggregates are considered by using two fractal dimensions of 1.8 and 2.8, and the fractal prefactor is fixed to be 1.2 [40]. The monomer diameter is assumed to be 30 nm, and two values of the refractive index m are considered, i.e., $1.4 + 0.6i$ and $1.8 + 0.6i$. The incident wavelength is fixed at 550 nm. For each set of parameters, five aggregates with different realizations will be averaged to smooth out the arbitrariness during aggregate generation. Exceptions to the above parameters for comparison with previously published simulations will be described separately. All simulations are carried out on a single node with 24 2.5 GHz processors and 128 GB memory.

Another advantage for this study is that a more efficient numerical solution for idealized aggregates of spheres exists. In particular, the MSTM code (v3.0) developed by Mackowski and Mishchenko [11,41] is used as a reference. While the MSTM is typically accurate to many digits for aggregates of a few spheres, its accuracy is not necessarily that good for aggregates of many spheres with large refractive index. This issue is complicated by several internal parameters controlling the accuracy, fine tuning of which is beyond the scope of this paper. We have, however, briefly tested another code based on the similar physical principles – the GMM. The difference between the MSTM and GMM (data not shown) do not exceed 1% even for larger aggregates, so we assume that as the upper bound of possible MSTM errors. This level is good enough for the final conclusion, since the typical DDA errors are significantly larger. The natural limitation of the MSTM is the assumption of aggregates of perfect spheres without overlapping, so, for more realistic cases, the DDA has to be applied.

3. The performance of the DDA

We first discuss the influence of spatial resolution, i.e., dpl, on the DDA simulation of aggregate optical properties, and decompose the influence of geometry representation on the DDA results. Fig. 1(a) shows a lacy aggregate (D_f=1.8) with 100 monomers. If the dpl, monomer size ($a = 15$ nm), and incident wavelength (550 nm) are given, the aggregates, i.e., all monomers, can be discretized into smaller dipoles. To better illustrate the discretization, only two of the 100 monomers are shown in the rest of the figure, and Fig. 1(c)–(e) are the two monomers discretized using different-sized dipoles with dpl of 50, 100, and 200. It is clearly shown that, with the increase of dpl, the monomers are better represented, and the overall discretized monomer becomes more spherical. The cubic elements are used to illustrate the dipoles since they correspond to the discrendtization scheme and facilitate further discussion of the errors. For those three cases, the DDA errors are introduced by two factors [34]. One is the numerical error related to the finite size of the dipole in comparison with the characteristic scale of the variation of the electric field inside the particle. The other reason is related to the difference between the real shape (Fig. 1(b)) and the shape represented by the dipoles (Fig. 1(c)–(e)), because the dipoles are defined solely by the location of their centers inside the monomers. For convenience, we refer the first kind of error as 'discretization error', and the second as 'shape error' [34]. The difference between a DDA result and 'exact' solution is referred to as 'total error', i.e., the combination of the two errors. With increasing dpl, the DDA accuracy is improved by both decreasing the discretization errors and giving better geometry representation. Note that all three errors can be negative or positive, so the amplitude of the total error is not necessary to be larger than those of its two components, which may cancel with each other.

Additional simulations are designed to separate errors of the two kinds, similarly to [35]. By increasing the dpl, the discretization error definitely decreases, whereas the shape errors of using a larger dpl may be retained. The geometry defined using larger dipoles, e.g., Fig. 1(c) with dpl = 50, can be re-discretized following its overall geometry using smaller dipoles, e.g., dpl = 200, resulting in Fig. 1(f). To keep the overall geometry, Fig. 1(f) uses smaller dipoles to represent the cubic space of each dipole in Fig. 1(c), and, with dpl increasing from 50 to 200 (i.e., kd decreasing from 0.12 to ~0.03), each dipole is further discretized into $(200/50)^3 = 64$ smaller ones (as illustrated by the green cubes from Fig. 1(c) to (f)). Strictly speaking, the discretization error for dpl = 50 is the difference between the DDA results for Fig. 1(c) and the limit of dpl $\to \infty$ for the same discretized shape [35]. Similarly, the shape error for dpl = 50 is the difference between the DDA results with

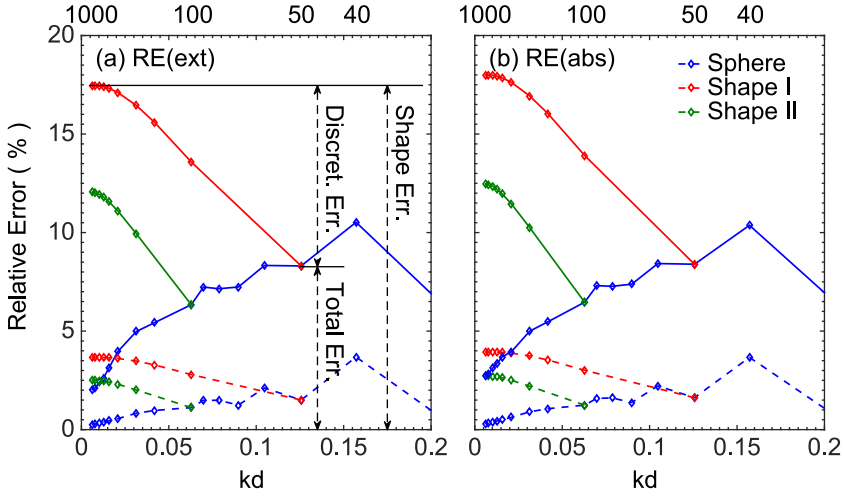

Fig. 2. Relative errors of the DDA results on the extinction and absorption of lacy BC aggregates with 100 monomers as functions of dipole size parameter (values of dpl are listed at the top axis). Solid lines are for aggregates with a refractive index of 1.8 + 0.6i, and dashed ones are for that of 1.4 + 0.6i. The monomers are either discretized with a full dipole resolution (sphere) or based on the coarser representations (Shape I and II).

the limit of dpl → ∞ for the discretized shape Fig. 1(c) and the exact solution for Fig. 1(b), and the latter can be obtained either by the MSTM or the DDA for the limit of dpl → ∞ for accurate spherical discretization. To be more specific, the discretization and shape errors for dpl = 50 can be approximated by the differences between DDA results of Fig. 1(f) and those of Fig. 1(c) and (e), respectively (note dpl of only 200, not ∞, is used for Fig. 1(e) and (f)).

Fig. 2 illustrates DDA errors for the aggregate in Fig. 1, and the REs of the DDA extinction (left) and absorption (right) from the MSTM results are shown. The extinction and absorption cross sections are compared, and we omit the "cross section" in the discussion of this study. The x-axis is given in the form of dipole size parameter *kd*, and the corresponding *dpl* values are listed in the top for reference. Note that the monomer size parameter for this case is *ka* = 0.17. Blue curves, discretizing the original spherical monomer, are for standard DDA simulations, and the REs decrease with the increase of *dpl* value. The red and green lines are for discussion on the shape errors. The solid and dashed lines are for aggregates with a refractive index of 1.8 + 0.6i and 1.4 + 0.6i, respectively. Here and further the results for extinction and absorption are similar, since absorption is much larger than scattering for most of the considered aggregates (small size and large Im(m)). Still we analyze both quantities as the most relevant ones for the experiments.

We discuss the results of m = 1.8 + 0.6i in Fig. 2 in details. Even with the *kd* reaching to ~0.006 (dpl = 1000), the DDA and MSTM still show relative difference of 2–3%. The origin of this residual is probably due to both the DDA and the MSTM (further discussed in Section 4). Anyway, it is small enough to make certain conclusions about the shape errors, which can be obtained by considering the red/green curves at small *kd*. For the red curves, during the increasing of the dpl, the particle is kept as the one discretized with a smaller dpl value of 50, i.e., the one illustrated by Fig. 1(c) (referred to as Shape-I). The green curves correspond to Shape-II that is initially discretized with a dpl of 100. As discussed above, with the decrease of dipole size, particle shape representation is not changed for the Shape-I and Shape-II, so the differences between the blue and red/green curves (especially, their values at dpl = 1000) can be understood as the shape errors of using a dpl of 50/100 for the DDA simulations. We can see that the REs for coarse shapes become almost constant as the *kd* becomes smaller than ~0.02 (or dpl > ~400), implying fast (at least quadratic) convergence of the discretization errors, similar to [34]. Nevertheless, for all shown curves the shape errors of the DDA simulations are approximately two times larger (and of opposite sign) than the discretization error for the same *kd*, since the sum of these two errors is the total error depicted by the blue curves (where it intersects with the red and green curve respectively). Meanwhile, at the other end of the blue curves, the DDA errors oscillate for simulations with large *kd* values (e.g. larger than ~0.15) that are even comparable to the monomer size parameter (e.g., *ka* = 0.17 here). Table 2 lists the corresponding errors of DDA simulations with dpl values of 50 and 100. We use the MSTM results as reference, and illustration in Fig. 2(a) can be used to understand how the errors are obtained. The results for 1.4 + 0.6i give much smaller REs but the same overall trends. This agrees with the previous study of single spheres [33], i.e., the DDA accuracy decreases as real part of refractive index increases. To summarize, large dpl is necessary to obtain satisfactory accuracy due to two reasons: (1) poor shape representation due to relatively small monomer size and (2) large real part of refractive index.

Let us take another look at the significant shape errors of the DDA simulations. The realistic BC aggregates are neither perfectly spherical nor point-to-point attached without overlapping as those defined in the MSTM, while the DDA discretization introduces imperfections to the idealized geometry. In other words, the discretized shapes defined in the DDA do differ from those defined in the MSTM, but are probably closer to realistic BC particles. Thus, the shape errors caused by DDA simulations with relatively small dpl could also be understood as an "advantage" of the DDA algorithm, although it lacks sufficient control for immediate application.

Conclusions of Fig. 2 seem to be significantly different from those given by some studies reviewed in Table 1 [22–28]. For example, Kahnert et al. and Wu et al. show that a dpl of ~40 is sufficient [22,24]. These differences are mainly caused by the presence of a relatively large coating sphere enclosing BC aggregates in their simulations. Fig. 3 gives an example of comparison with those given by Wu et al. [24]. The REs of the DDA simulations for aggregates with and without non-absorptive coating sphere are illustrated here. Most parameters are assumed to be the same as those used in Wu et al. [24], in contrast to the rest of this manuscript. The radii of coating spherical particle and monomer are 300 nm and 20 nm, respectively. The aggregates have 50 and 100 monomers. However, the general conclusions will not change. The refractive indices of BC and coating are 1.76 + 0.57*i* and

Table 2
List of typical relative errors (in percents) of the DDA simulations of the extinction of BC aggregates as those illustrated in Fig. 2.

dpl	*kd*	1.4 + 0.6i			1.8 + 0.6i		
		Discretization	Shape	Total	Discretization	Shape	Total
50	0.13	−2.2	3.7	1.5	−9.2	17.5	8.3
100	0.06	−1.4	2.5	1.1	−5.8	12.1	6.3

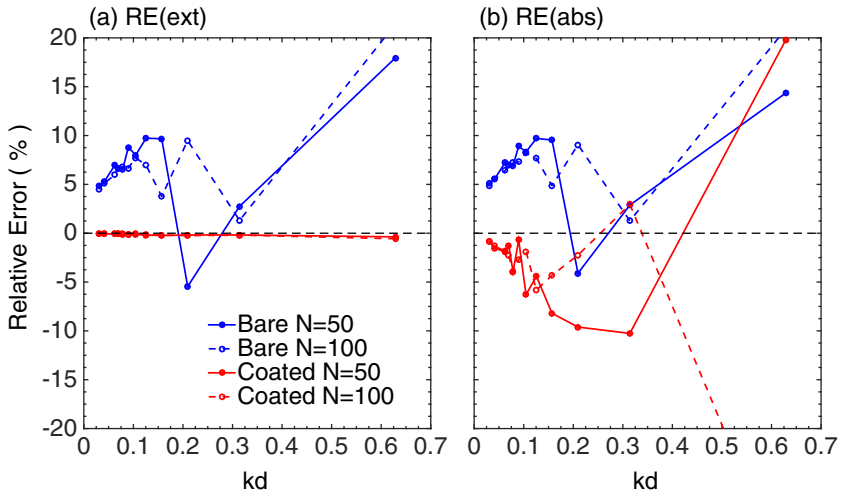

Fig. 3. The relative errors of extinction and absorption between the DDA and MSTM as functions of dpl for the same aggregates as considered in Wu et al. [24]. (see text for details).

$1.44 + 0i$ at the incident wavelength of 670 nm. The fractal dimension is 2.5. For aggregates with coating, the DDA REs become less than 2% (for both extinction and absorption) as the *kd* becomes smaller than 0.06 (the extinction errors are almost zero at almost all *kd* values), while there are significant remaining errors for the non-coating cases (discussed in Section 4). Because the large coating sphere is the dominant component for the coating cases, the influence of monomer structure becomes less important with aggregate volume fraction being less than 5%. Furthermore, obvious oscillations are noticed for *kd* larger than 0.1. To conclude, the dpl should be carefully chosen for DDA simulations of aggregates with small-scale monomers.

Results in Figs. 2 and 3 are averaged for randomly oriented aggregates, which raise another key difference between the DDA and MSTM, i.e., the methods for scattering simulations of randomly oriented particles. The DDA has to be applied multiple times for numerical averaging over different particle orientations, while the MSTM calculates them analytically in one simulation. Thus, the number of orientations needed to obtain the optical properties of randomly oriented aggregates is also important for the efficiency of DDA simulation. Fig. 4 shows the REs of the extinction (red), absorption (blue), and scattering (green) and asymmetry factor (purple) of aggregates given by the DDA as a function of the number of orientations used for averaging. Both lacy and compact aggregates ($D_f = 1.8$ and 2.8) with $m = 1.8 + 0.6i$ and $N = 100$ are illustrated here, and a dpl value of 300 is used for the simulation. The results show little variation over the number of orientations performed. The variations are smaller for compact structures with $D_f = 2.8$, because they have a more spherical overall geometry and are less sensitive to orientation. There are slight oscillations on the REs when the number of orientation is small, but their values are mostly under 10%. After the orientation number becoming larger than 32, the REs become almost constant, which is expected since the aggregates overall size is relatively small. Considering that the scattering properties of BC aggregates are less sensitive to particle orientations, the default convergent rule used in the ADDA implementation is used in the following simulations, and normally 64–128 independent orientations are used. The results for aggregates with other sizes (N or a) are similar, and will not be presented.

Fig. 5 shows the REs of extinction, absorption, and asymmetry factor (g), and the ratio of computational time of DDA simulations to those of the corresponding MSTM, and the results are for aggregates with a fixed/single orientation and random orientations. Again, we consider both lacy and compact aggregates but with monomer numbers from 10 to 1000, $m = 1.8 + 0.6i$, and dpl = 200. For extinction and absorption, the REs decrease as the monomer number increases, especially for compact aggregates, and are generally under 5%. Similarly, the REs on asymmetry factor can converge to 2% and 0% for lacy and compact aggregates as the particle size increases, respectively, whereas the REs are much larger when the aggregates are small. The results for fixed and randomly oriented aggregates are almost the same. For the computational efficiency, the MSTM is approximately one order of magnitude faster than the DDA for compact aggregates, and two orders of magnitude faster for lacy aggregates.

Table 3 lists the computational resources used for the simulations, i.e. the memory and computational time, and only those for lacy aggregates are included. As expected, the memory usage and computational time are sensitive to particle size. For the MSTM, the differences between memory usages required for different-sized particles are relatively small. However, the memory usages of the DDA substantially increase as the monomer number increases. For example, the memory required for aggregates with 1000 monomers is approximately three orders of magnitude larger than that for aggregates with 10 monomers. Thus, the memory requirements of the DDA in most cases are much larger than those of the MSTM, but still within the range of current computational capabilities. The computational times of the MSTM and DDA for aggregate with 10 monomers at a fixed origination are two or-

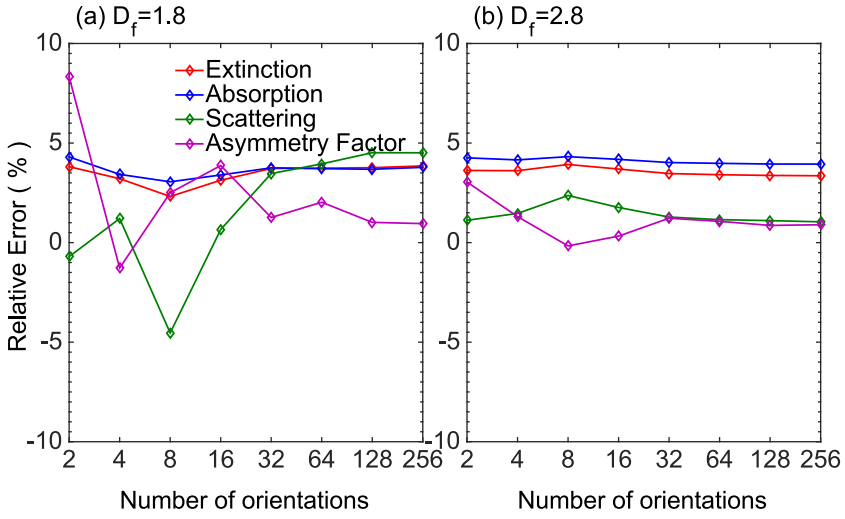

Fig. 4. Relative errors of the extinction (red), absorption (blue), scattering (green), and asymmetry factor (purple) of randomly oriented aggregates with lacy (a) and compact (b) structures and 100 monomers ($m = 1.8 + 0.6i$) as a function of number of orientations. (For interpretation of the references to color in this figure legend, the reader is referred to the web version of this article.)

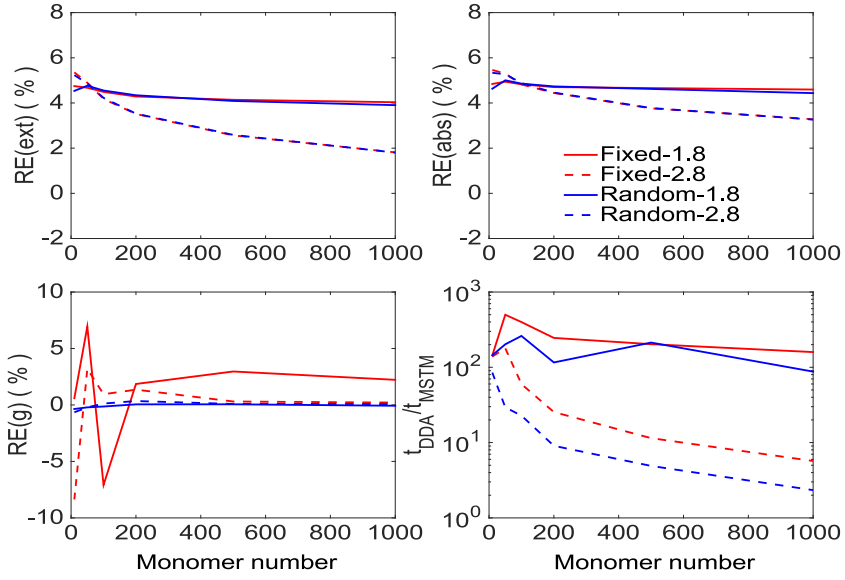

Fig. 5. Relative errors of extinction, absorption, and asymmetry factor, and ratio of computational times of the DDA to the MSTM for fixed and randomly orientated aggregates ($m = 1.8 + 0.6i$).

Table 3
Memory and computational time (in second) of the MSTM and DDA for different-sized lacy aggregates with $m = 1.8 + 0.6i$.

N	Fixed orientation				Random orientation			
	Memory (MB)		Time (s)		Memory (MB)		Time (s)	
	MSTM	DDA	MSTM	DDA	MSTM	DDA	MSTM	DDA
10	156	48	<0.01	1.4×10^{0}	158	52	3.6×10^{-2}	5.2×10^{0}
50	158	458	1.0×10^{-2}	5.0×10^{0}	166	463	5.6×10^{-1}	1.1×10^{2}
100	158	1331	3.6×10^{-2}	1.4×10^{1}	183	1331	2.7×10^{0}	7.1×10^{2}
200	158	2970	1.3×10^{-1}	3.2×10^{1}	226	3072	1.3×10^{1}	1.5×10^{3}
500	165	14,336	7.7×10^{-1}	1.6×10^{2}	304	14,336	1.1×10^{2}	2.2×10^{4}
1000	182	38,912	3.1×10^{0}	5.0×10^{2}	333	38,912	6.6×10^{2}	5.8×10^{4}

ders of magnitude faster than those with 1000 monomers, and the ratio becomes four orders magnitude for random orientation cases. However, the computational times much less than one second should quite sensitive from case to case, and may have some errors. The results of compact aggregates are similar to those of lacy aggregates, except that the DDA and MSTM computational times are much shorter than those shown in Table 3, and the results will not be given here.

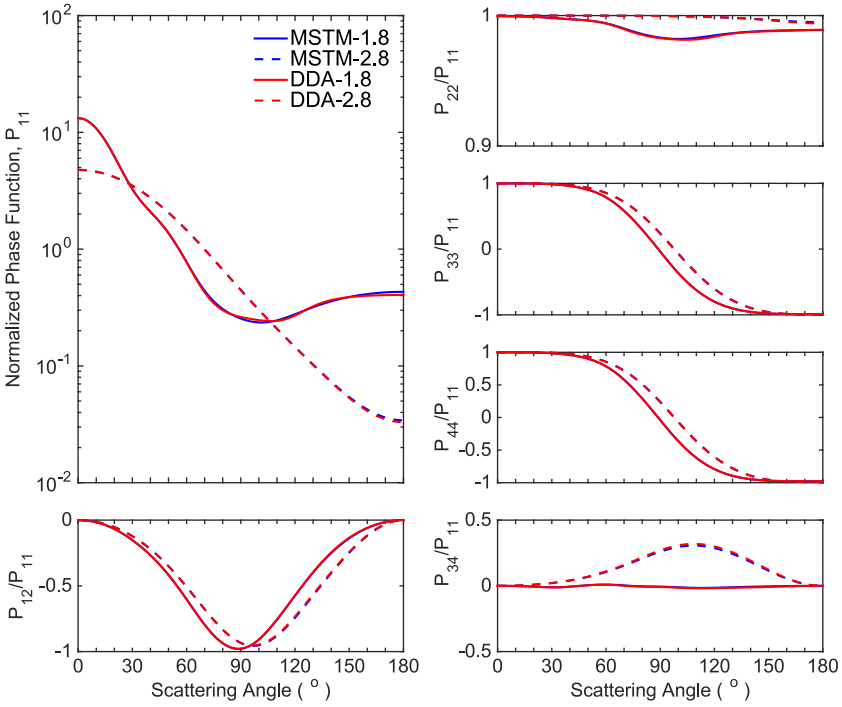

Fig. 6. Comparison of the non-zero scattering matrix elements of aggregates with 400 monomers.

Fig. 6 shows the scattering matrix elements of lacy and compact aggregates with 400 monomers. The agreement for the MSTM and DDA results on the scattering matrix elements is excellent, and only slight differences are noticed at backward scattering for lacy aggregates. Fig. 6 shows that, besides the phase function, P_{22}/P_{11} and P_{34}/P_{11} are slightly sensitive to the fractal dimension, whereas other elements are essentially unaffected. Note that this is the only scattering matrices that we illustrate in this study, because the great agreement is given by the two methods, and current applications related to BC optical properties are more interested in the integral scattering properties discussed above.

Most previous results are based on the refractive index of $1.8+0.6i$, whereas the simulations are sensitive to the refractive index as well, especially for the DDA [33]. Furthermore, the refractive index is always one of the most uncertain aerosol properties, because it cannot be measured directly. To study the effects of BC refractive index on the DDA performance, Fig. 7 shows the REs of extinction, absorption, and asymmetry factor, and the DDA efficiency relative to the MSTM at different refractive indices. The results are for lacy aggregates with 100 monomers. A small dpl of 100 is used, because we mainly consider relative efficiency, not accuracy. As a result, the ratios of the computational times shown in the figure can be quite different from those of Fig. 5 and Table 3, which use a dpl of 200. The REs on the extinction and absorption clearly increase as real part increases, and are less sensitive to the imaginary part. The REs for the asymmetry factor are much smaller, i.e. within 2%, and do not show any trends over the refractive indices. For the computational time, the ratios of the DDA to MSTM increase slightly as the real part or imaginary part of refractive index increases, but are always in the same order with values around 20. Again, the figure indicates that higher spatial resolution is necessary for DDA simulations of aggregates because of the relatively large real parts of BC refractive indices.

4. DDA with effective medium approximation

As indicated by Fig. 2 and results discussed above, the difficulties of applying the DDA for aggregates are mainly caused by discretization of the monomers that are significantly smaller than the wavelength. Thus, really small dipole size has to be used to represent the spherical structures of monomers (dpl up to a few hundreds). This can be clearly shown by the two-dimensional illustration in Fig. 8. The blue grids indicate dipoles, and the red circles are the monomers in two dimensions. In the left panel of Fig. 8, grids inside the circle are shown in black, and the circle cannot be well described by the coarse dipoles/grids at all. Most dipoles located at circular edge can only be defined as either particle or vacuum determined by their centers. This poor representation is a common problem for methods discretizing the space domain such as the FDTD. Yang and Liou [42] introduce the effective medium approximation (EMA) to redefine the grids on particle edge in the FDTD simulations to eliminate the numerical errors. This has also been discussed in the framework of the DDA as the “weighted discretization” [34,43]. The right panel of Fig. 8 shows the idea of applying the EMA for light scattering simulations. For a ‘dipole’ at the edge, a part of it is inside the monomer, while the other part is vacuum. Thus, those dipoles can be defined as materials between the original material and vacuum depending on the volume fraction, and the darkness of those grids illustrates the corresponding volume fraction, or refractive indices. With the gray dipoles introduced, there is a smooth transition between the BC material and the vacuum space, so it is expected to give more accurate representation on the particle geometries with even relatively large dipoles.

The idea of the combination of the DDA and EMA (without modification of the existing code) is to use multiple refractive indices, instead of only a single one of BC, to define the dipoles on particle edge, whereas the choice of a particular EMA rule is

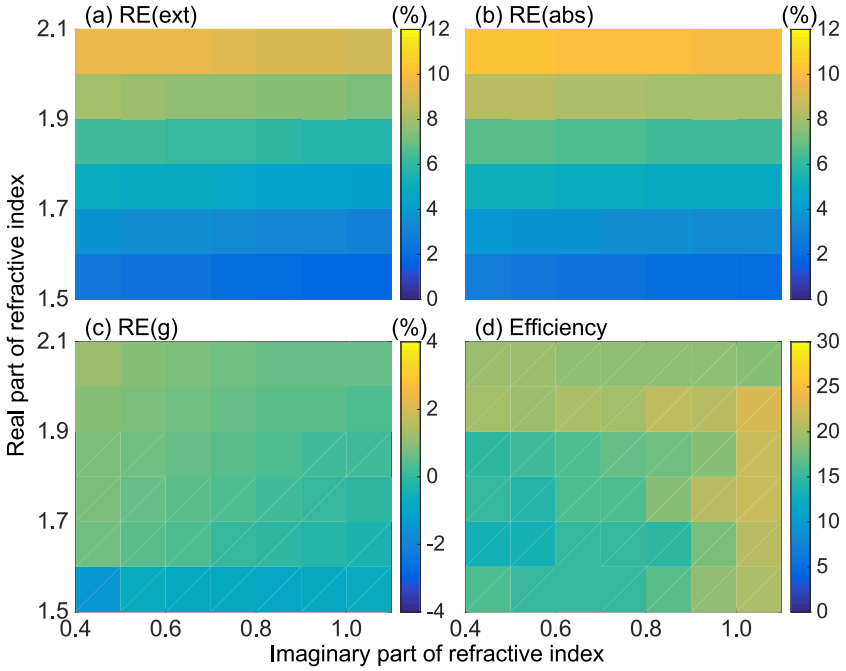

Fig. 7. Relative errors of extinction, absorption, and asymmetry factor, and computational efficiency (given by the ratio of computational times of the DDA to the MSTM) for aggregates with different refractive indices.

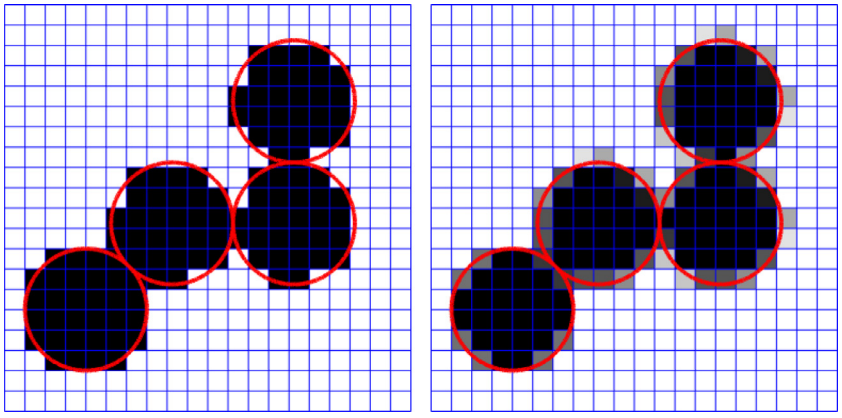

Fig. 8. Illustration of the DDA discretization using small dipoles in two domains.

ambiguous. There are numerous approximations to give the effective refractive index of mixtures [44], and two of the most popular and general ones, namely the Maxwell-Garnett (MG) and Bruggeman (BR) theory, are tested. The refractive indices of the two methods are given by:

$$\frac{m_{MG}^2 - m_2^2}{m_{MG}^2 + 2m_2^2} = f_1 \frac{m_1^2 - m_2^2}{m_1^2 + 2m_2^2} \tag{2}$$

$$f_1 \frac{m_1^2 - m_{BR}^2}{m_1^2 + 2m_{BR}^2} + f_2 \frac{m_2^2 - m_{BR}^2}{m_2^2 + 2m_{BR}^2} = 0 \tag{3}$$

Here, m_1 and m_2 are the refractive indices of two components of the mixture (BC and vacuum in this study), and their corresponding volume fractions in each dipole are f_1 and f_2, respectively. The two materials in the BR are symmetric, and there is no difference on which is defined as m_1 or m_2. Note that the two materials with m_1 and m_2 in the MG are asymmetric, and they are understood as the inclusion and host/medium, respectively. Theoretically, the fraction of the inclusion f_1 should be small [44]. However, we have to treat BC, i.e., m_1, as inclusion independent of the value of f_1 or f_2, and $m_2 = 1$ for vacuum is the host/medium. Only in this way the polarizability of point dipoles in the DDA, determined by the volume-weighted $\frac{m^2-1}{m^2+2}$, becomes the same for a homogeneous dipole with m_{MG} and an inhomogeneous dipole with BC volume fraction being f_1. To be more specific, with $m_2 = 1$, we have the polarizability of the inhomogeneous dipole given by:

$$f_1 \frac{m_1^2 - 1}{m_1^2 + 2} + f_2 \frac{m_2^2 - 1}{m_2^2 + 2} = f_1 \frac{m_{BC}^2 - 1}{m_{BC}^2 + 2} = \frac{m_{avg}^2 - 1}{m_{avg}^2 + 2} \tag{4}$$

which is the same as Eq. (2) (m_{avg}, the average refractive index to give the same volume-averaged polarizability, equals to m_{BC}).

Fig. 9 compares the refractive indices given by the two EMAs, and the BC refractive index is assumed to be $1.8 + 0.6\mathrm{i}$. Both real and imaginary parts of refractive indices increase gradually from that of vacuum to the BC value we used. The real parts of refractive index given by the MG and BR are almost coincident, whereas the MG gives smaller imaginary parts than those from the BR. During discretization, we additionally discretize each dipole to determine the volume fraction of BC, and then the corresponding effective refractive index can be given following Eq. (2) or (3).

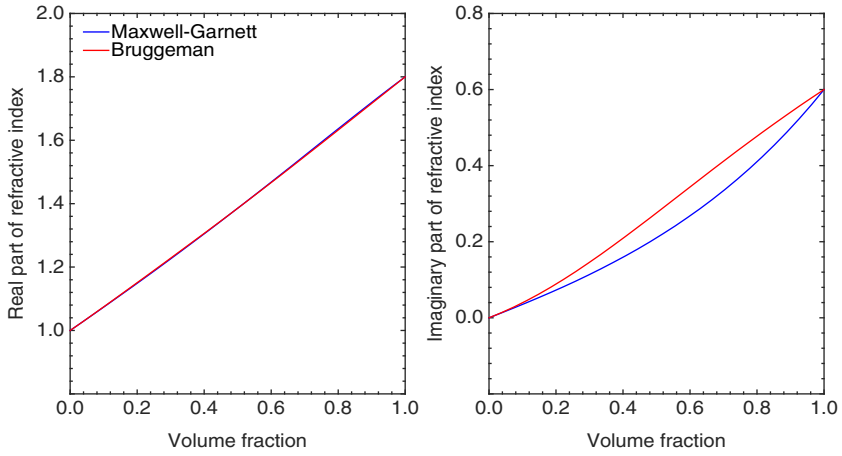

Fig. 9. Comparison of refractive indices given by the two effective medium approximations.

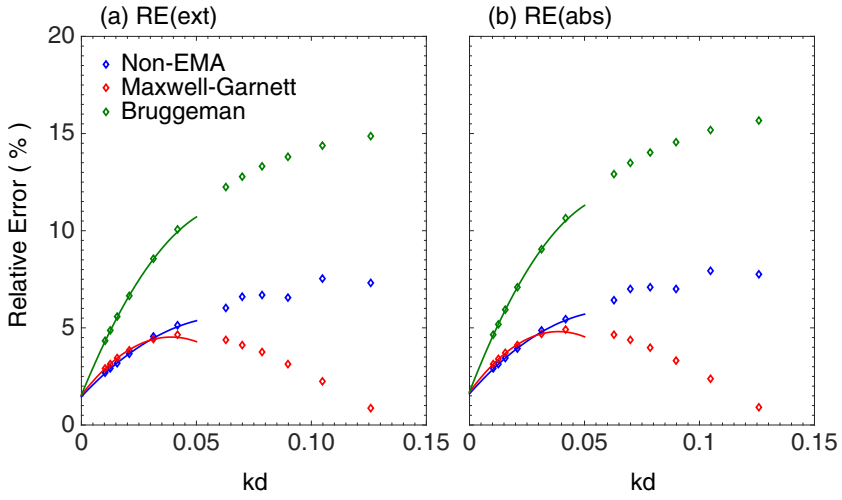

Fig. 10. Comparison of the extinction and absorption of lacy BC aggregates with 100 monomers between the DDA simulations with and without the EMA treatment. Markers are the DDA results, and the solid lines are quadratic fits for the DDA results.

Fig. 10 compares DDA results with and without applying the EMA, and the same aggregates used for Fig. 2 with the refractive index of $1.8+0.6i$ are considered. The blue markers are the results presented in Fig. 2 for simulations without applying the EMA, and the red and green markers are for DDA with the MG and BR, respectively. With the EMA, the REs given by DDA become much more smooth at large kd values (or small dpl), because, as illustrated by Fig. 8, the geometry of BC monomers can be better and more smoothly represented. Furthermore, the DDA + MG results give smaller REs than those of original DDA when kd is larger than 0.05, and the two results become comparable for small kd. The great performance of the MG may be due to the correct value of the volume-averaged $\frac{m^2-1}{m^2+2}$ (which largely determines absorption for those aggregates) after redefining the edge dipoles. By contrast, the DDA + BR makes the relative errors even larger, probably due to the different imaginary part of the effective refractive index.

First obvious advantage of using MG EMA is significant enhancement of the simulation efficiency for practical applications by applying much smaller dpl (keeping the satisfactory accuracy). Second advantage is not that obvious, but is fundamentally more important. The convergence curves of DDA + EMA are very smooth, inviting the use of Richardson-style extrapolation down to $kd=0$. As the simplest example we follow the empirical procedure proposed in [35], these particles also have smooth convergence curves due to the absence of shape errors. We take 6 best discretization ($kd \leq 0.05$) and fit a quadratic function through them, assuming that the expected fit errors are proportional to $(kd)^3$, i.e. weights for the squared residuals are $(kd)^{-6}$. The obtained standard error for the zero-th polynomial coefficient of the fit, i.e. its value at $kd=0$ is multiplied by 2 to obtain reasonable (nominal 95%) confidence interval given quasi-random remaining shape errors. The natural way is to fit the results of DDA simulations (extinction, absorption, etc.), but here we apply this idea directly to the relative errors (differences) shown in Fig. 10, since they are linearly connected with the original data.

The resulting quadratic fits are also shown in Fig. 10 by the solid lines, they pass very close to the original points used for the fit. The confidence ranges for extinction (the relative difference with the MSTM) are $(1.532 \pm 0.052)\%$ and $(1.536 \pm 0.053)\%$ for MG and BR, respectively. The agreement between them is surprisingly good, considering the large difference between the original convergence curves. Moreover, the agreement is even better than the fit uncertainties, suggesting that we may be over-estimating the uncertainty (recall that the extrapolation procedure is largely empirical). The original data for the DDA without EMA lie in confidence range of $(1.46 \pm 0.13)\%$ – significantly different but consistent with the above ones. Larger uncertainties of the non-EMA results correspond to their less smooth convergence curve as discussed above. The results for absorption are similar – $(1.691 \pm 0.056)\%$, $(1.697 \pm 0.059)\%$, and $(1.60 \pm 0.13)\%$ for the MG, BR, and non-EMA,

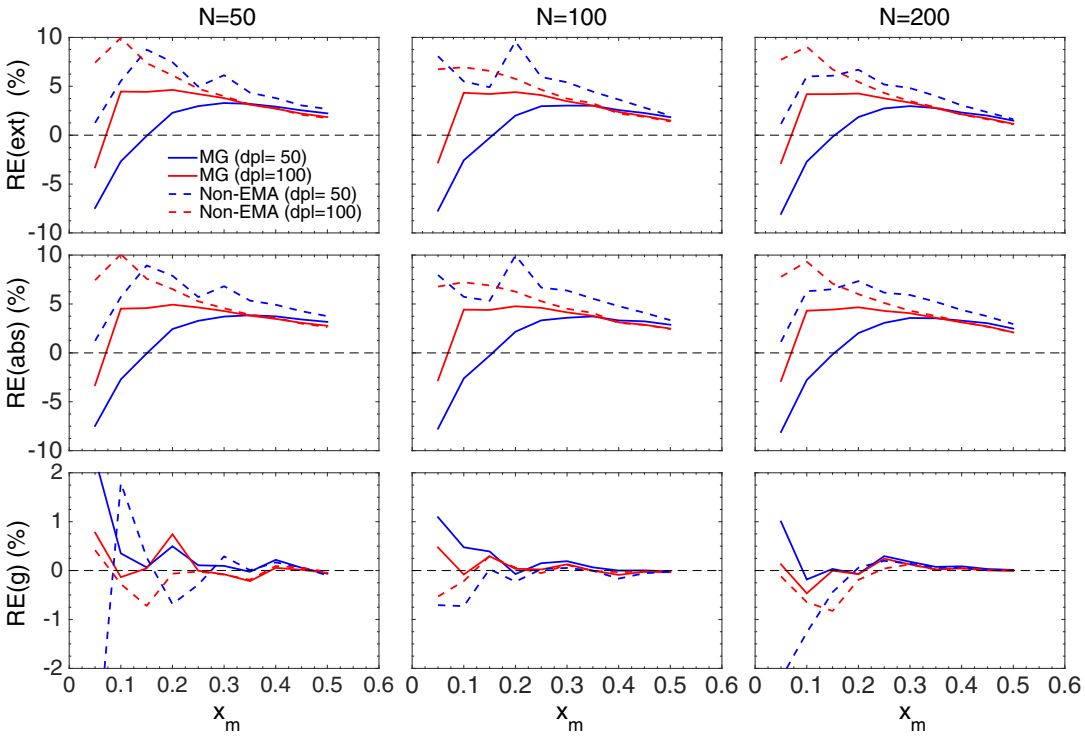

Fig. 11. Relative errors of the extinction, absorption, and asymmetry factors given by the DDA simulations with and without the EMA treatment at different aggregate and monomer sizes. The three columns from left to right are for aggregates with 50, 100, and 200 monomers.

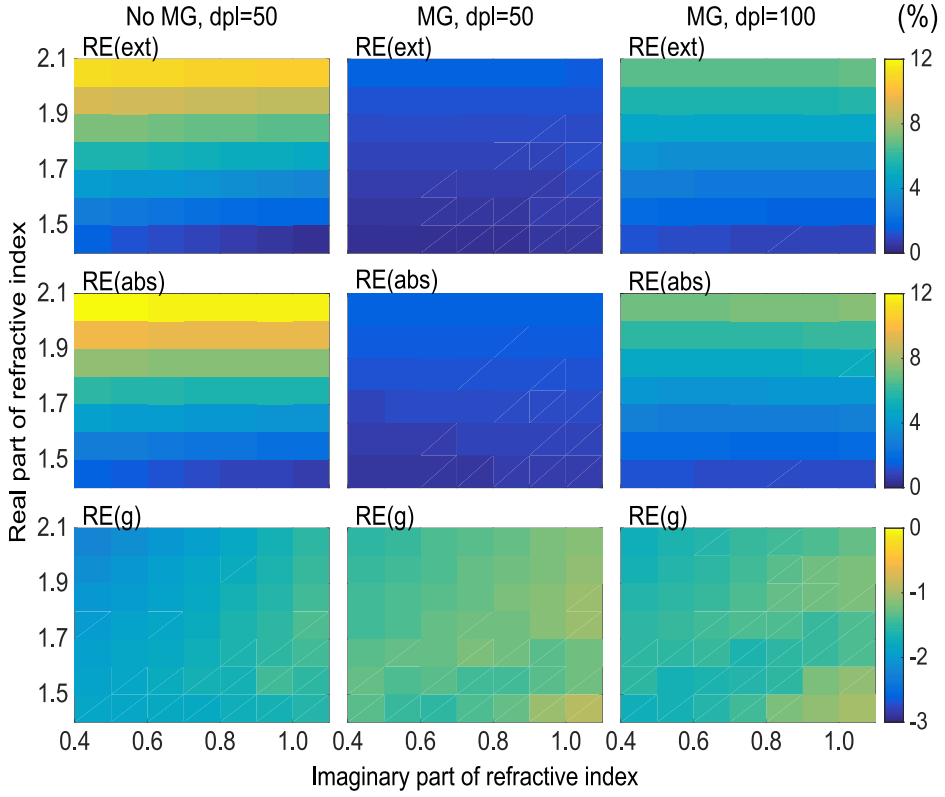

Fig. 12. Relative errors of the extinction, absorption, and asymmetry factors given by the DDA simulations with (middle and right) and without (left) the EMA treatment at different refractive indices.

respectively. Even accounting for some uncertainty due to orientation averaging ($\leq$ 0.5%), this analysis strongly suggests that the reference MSTM result may have the error of approximately 1%. However, a more systematic analysis of the latter, including variation of all its internal parameters, is required to make definite conclusions. We leave such analysis for a future research.

The single case in Fig. 10 indicates the possibility of improving both DDA accuracy and efficiency by applying the MG for discretization, while its general performance for practical applications under different circumstances are unclear. Fig. 11 compares the REs given by the DDA simulations with and without the MG for BC particles with different monomer and aggregate sizes, and the dpl values of 50 and 100 are used for the simulation. The x-axis is for monomer size parameter, i.e., $x_m = 2\pi a/\lambda$, from 0.05 to 0.5, and three aggregate sizes with $N = 50$, 100, and 200 are illustrated from left to right. The DDA simulations with and without applying the MG show quite different errors for aggregates with small-sized monomers, and their results become similar for x_{m} larger than ~0.35 for simulations using a dpl of 100. The DDA + MG errors on the extinction and absorption are mostly under 5% at dpl of both 50 and 100, whereas those without the MG have REs as large as 10%. Again, the asymmetry factors show much smaller REs, mostly less than 1%. Furthermore, the DDA + MG shows almost the same results for the three aggregate sizes considered, whereas those for DDA without the MG are slightly different. Overall, Fig. 11 indicates that the application of the MG in most cases improves the accuracy of the DDA. The improvement is largest when a few dipoles fit along the monomer diameter. For larger monomers the original discretization is already fine, while for smaller monomers all dipoles are boundary ones and the averaging can even be detrimental. For cases considering very small monomers, e.g. Zhang et al. [45] observed monomer radii of ~7.5 nm (x_m less than 0.1 at visible wavelengths), the original application of the DDA can be really dangerous unless using a very large dpl, whereas the DDA + MG can give reasonable results using dpl of even less than 100.

Last but not the least, the performance of the DDA + MG for aggregates with different refractive indices is illustrated in Fig. 12, and the aggregate parameters are the same as those used for Fig. 7. The left panels are for simulations with a dpl value of 50 and without the EMA, and the middle and right ones are for those with the EMA and dpl of 50 and 100, respectively. Application of the MG during the discretization systematically reduces the errors from more than 10% to several percent at a dpl of 50 at all refractive indices in the figure, i.e., typical BC values. Considering both the results in Figs. 11 and 12, the errors for DDA + MG with dpl values of 50 and 100 are in similar ranges, so, instead of dpl values of a few hundred suggested by the previous section, values in the order of a few tens become sufficient for the DDA + MG.

To summarize, our first attempt of application of the MG to determine the refractive index of the boundary dipoles shows great promise as it systematically enhances DDA performance for simulations of aggregates with monomer size smaller than the wavelength due to the better representation of aggregate geometry with even relatively smaller dpl. The improvements on both accuracy and efficiency make the DDA a more powerful tool to study BC optical properties, especially when applied to more realistic aggregate geometries. However, further work is required for a broad application of those ideas. First, more advanced existing formulations for the weighted discretization [46] should be implemented in a mature DDA code, such as ADDA, and tested for a broad range of problems. Second, the extrapolation technique should be also broadly tested, when applied together with different weighted discretization and DDA formulations, such as the IGT.

5. Conclusion

This paper systematically investigates the performances of the DDA on simulating the optical properties of BC aggregates, using the MSTM as a reference. Different from the well-known assignment of dipole size, i.e. about 10 times smaller than the incident wavelength, much larger dpl values are necessary for this particular case of BC aggregates with small-sized monomers. The DDA relative errors can be limited to less than 5% if the dpl is increased to over 200 at typical BC refractive indices. A significant part of the DDA error is due to the poor discretized representation of particle shape with structures much smaller than the incident wavelength, whereas such differences (over 10% at a dpl of 100) may also be understood as an advantage of the DDA for accounting for imperfect geometries of BC aggregates. Although the DDA and MSTM apply totally different approaches to obtain optical properties of randomly oriented particles, their relative efficiency is not affected by the simulations for a fixed orientation or random orientations. To alleviate the abovementioned shape errors, we introduce the EMA for better particle discretization, which defines the refractive indices of dipoles on particle edge based on the volume fraction inside the particle. This leads to the DDA errors under 5% with a dipole size parameter of 0.1 or even larger (dpl of a few tens). The treatment should definitely be applied for further DDA simulations of aggregate optical properties, although there are a few ideas for its further improvement. Moreover, combined with the extrapolation to $kd \to 0$, the EMA has a potential for very accurate DDA results, similar to those for cubes [46] and surpassing that of the MSTM reference.

Acknowledgments

We thank Daniel W. Mackowski and Michael I. Mishchenko for their MSTM code. This study is supported by the National Natural Science Foundation of China (NSFC) (41505018 and 41475005), Young Elite Scientists Sponsorship Program by CAST (2017QNRC001), Russian Science Foundation (18-12-00052), and National Supercomputer Center in Guangzhou (NSCC-GZ).

Supplementary materials

Supplementary material associated with this article can be found, in the online version, at doi:10.1016/j.jqsrt.2018.09.030.

References

[1] Ramanathan V, Carmichael G. Global and regional climate changes due to black carbon. Nat Geosci 2008;1:221–7.
[2] Ding A, Huang X, Nie W, Sun J, Kerminen VM, et al. Enhanced haze pollution by black carbon in megacities in China. Geophys Res Lett 2016;43:2873–9.
[3] Chakrabarty RK, Moosmüller H, Garro MA, Arnott WP, Walker J, Susott RA, Hao WM. Emissions from the laboratory combustion of wildland fuels: particle morphology and size. J Geophys Res Atmos 2006;111. doi:10.1029/2005JD006659.
[4] Wang Y, Liu F, He C, Bi L, Cheng T, et al. Fractal dimensions and mixing structures of soot particles during atmospheric processing. Environ Sci Technol Lett 2017;4(11):487–93.
[5] Sorensen CM. Light scattering by fractal aggregates: a review. Aerosol Sci Tech 2001;35:648–87.
[6] Kahnert M, Devasthale A. Black carbon fractal morphology and short-wave radiative impact: a modeling study. Atmos Chem Phys 2011;11:11745–59.
[7] Liu L, Mishchenko MI. Scattering and radiative properties of complex soot and soot-containing aggregate particles. J Quant Spectrosc Radiat Transfer 2007;106:262–73.
[8] Liu L, Mishchenko MI. Effects of aggregation on scattering and radiative properties of soot aerosols. J Geophys Res Atmos 2005;110. doi:10.1029/2004JD005649.
[9] Liu F, Smallwood GJ. Radiative properties of numerically generated fractal soot aggregates: the importance of configuration averaging. J Heat Transfer 2010;132. doi:10.1115/1.4000245.

[10] Smith AJA, Grainger RG. Simplifying the calculation of light scattering properties for black carbon fractal aggregates. Atmos Chem Phys 2014;14:7825–36.
[11] Mackowski DW. A general superposition solution for electromagnetic scattering by multiple spherical domains of optically active media. J Quant Spectrosc Radiat Transfer 2014;133:264–70.
[12] Xu YL. Electromagnetic scattering by an aggregate of spheres. Appl Opt 1995;34:4573–88.
[13] Chung C, Lee K, Mueller D. Effect of internal mixture on black carbon radiative forcing. Tellus B 2013;64(1). doi:10.3402/tellusb.v64i0.10925.
[14] Draine BT, Flatau PJ. Discrete-dipole approximation for scattering calculations. J Opt Soc Am A 1994;11:1491–9.
[15] Yurkin MA, Hoekstra AG. The discrete dipole approximation: an overview and recent developments. J Quant Spectrosc Radiat Transfer 2007;106:558–89.
[16] Yang P, Liou KN. Finite-difference time domain method for light scattering by small ice crystals in three-dimensional space. J Opt Soc Am A 1996;13:2072–85.
[17] Liou KN, Takano Y, Yang P. Light absorption and scattering by aggregates: application to black carbon and snow grains. J Quant Spectrosc Radiat Transfer 2011;112:1581–94.
[18] He C, Takano Y, Liou KN, Yang P, Li Q, Mackowski DW. Intercomparison of the GOS approach, superposition T-matrix method, and laboratory measurements for black carbon optical properties during aging. J Quant Spectrosc Radiat Transfer 2016;184:287–96.
[19] Yon J, Bescond A, Liu F. On the radiative properties of soot aggregates part 1: necking and overlapping. J Quant Spectrosc Radiat Transfer 2015;162:197–206.
[20] Skorupski K, Mroczka J. Effect of the necking phenomenon on the optical properties of soot particles. J Quant Spectrosc Radiat Transfer 2014;41:40–8.
[21] Skorupski K, Mroczka J, Riefler N, Oltmann H, Will S, Wriedt. Impact of morphological parameters onto simulated light scattering patterns. J Quant Spectrosc Radiat Transfer 2013;119:53–66.
[22] Kahnert M, Nousiainen T, Lindqvist H, Ebert M. Optical properties of light absorbing carbon aggregates mixed with sulfate: assessment of different model geometries for climate forcing calculations. Opt. Express 2012;20(9):10042–58.
[23] Prasanna S, Rivière P, Soufiani A. Effect of fractal parameters on absorption properties of soot in the infrared region. J Quant Spectrosc Radiat Transfer 2014;148:141–55.
[24] Wu Y, Cheng T, Zheng L, Chen H, Xu X. Single scattering properties of semi-embedded soot morphologies with intersecting and non-intersecting surfaces of absorbing spheres and non-absorbing host. J Quant Spectrosc Radiat Transfer 2015;157:1–13.
[25] Moteki N. Discrete dipole approximation for black carbon-containing aerosols in arbitrary mixing state: a hybrid discretization scheme. J Quant Spectrosc Radiat Transfer 2016;178:306–14.
[26] Liu C, Li J, Yin Y, Zhu B, Feng Q. Optical properties of black carbon aggregates with non-absorptive coating. J Quant Spectrosc Radiat Transfer 2017;187:443–52.
[27] Doner N, Liu F, Yon J. Impact of necking and overlapping on radiative properties of coated soot aggregates. Aerosol Sci Tech 2017;51(4):532–42.
[28] Tazaki R, Tanaka H. Light scattering by fractal dust aggregates. II. opacity and asymmetry parameter. Astrophy J 2018;860(1). doi:10.3847/1538-4357/aac32d.
[29] Jain P, Eustis S, El-Sayed MA. Plasmon coupling in nanorod assemblies: optical absorption, discrete dipole approximation simulation, and exciton-coupling model. J Phys Chem B 2006;110:18243–53.
[30] Amendola V, Bakr OM, Stellacci F. A study of the surface plasmon resonance of silver nanoparticles by the discrete dipole approximation method: effect of shape, size, structure, and assembly. Plasmonics 2010;5(1):85–97.
[31] Lumme K, Rahola J. Light scattering by porous dust particles in the discrete-dipole approximation. Astrophys J 1994;425:653–67.
[32] Ori D, Kneifel S. Assessing the uncertainties of the discrete dipole approximation in case of melting ice particles. J Quant Spectrosc Radiat Transfer 2018;217:396–406.
[33] Liu C, Bi L, Panetta RL, Yang P, Yurkin MA. Comparison of the pseudo-spectral time domain method and the discrete dipole approximation for light scattering simulations. Opt Express 2012;20:16763–76.
[34] Yurkin MA, Maltsev VP, Hoekstra AG. Convergence of the discrete dipole approximation. I. Theoretical analysis. J Opt Soc Am A 2006;23:2578–91.
[35] Yurkin MA, Maltsev VP, Hoekstra AG. Convergence of the discrete dipole approximation. II. An extrapolation technique to increase the accuracy. J Opt Soc Am A 2006;23:2592–601.
[36] Yurkin MA, Hoekstra AG. The discrete dipole approximation: an overview and recent developments. J Quant Spectrosc Radiat Transfer 2007;106:558–89.
[37] Yurkin MA, Hoekstra AG. User manual for the discrete dipole approximation code ADDA 1.3 b4; 2014. https://github.com/adda-team/adda.
[38] Smunev DA, Chaumet PC, Yurkin MA. Rectangular dipoles in the discrete dipole approximation. J Quant Spectrosc Radiat Transfer 2015;156:67–79.
[39] Filippov AV, Zurita M, Rosner DE. Fractal-like aggregates: relation between morphology and physical properties. J Colloid Interface Sci 2000;229(1):261–73.
[40] Sorensen CM, Roberts GC. The prefactor of fractal aggregates. J Colloid Interface Sci 1997;186:447–52.
[41] Mackowski DW, Mishchenko MI. Calculation of the T-matrix and the scattering matrix for ensembles of spheres. J Opt Soc Am A 1996;13:2266–78.
[42] Yang P, Liou KN. Light scattering by hexagonal ice crystals: comparison of finite-difference time domain and geometric optics models. J Opt Soc Am A 1995;12:162–76.
[43] Piller NB. Influence of the edge meshes on the accuracy of the coupled-dipole approximation. Opt Lett 1997;22:1674–6.
[44] Lucarini V, Saarinen JJ, Peiponen KE, Varitiainen EM. Kramers-Kronig relations in optical materials. Heidelberg: Springer; 2014.
[45] Zhang R, Khalizov AF, Pagels J, Zhang D, Xue X, McMurry P. Variability in morphology, hygroscopicity, and optical properties of soot aerosols during atmospheric processing. Proc Natl Acad Sci USA 2008;105:10291–6.
[46] Yurkin MA, Kahnert M. Light scattering by a cube: accuracy limits of the discrete dipole approximation and the T-matrix method. J Quant Spectrosc Radiat Transfer 2013;123:176–83.